# Chaotic Mixing

Chaos and Dynamical Systems

Scott Malley

May 15, 2015

# 1 Introduction

Fluid mixing is an important technical consideration when combining two different fluids in any circumstance. Often in applications we want to know how effectively or thoroughly a fluid is mixed. To do this we can consider areas of the fluid that remain constant before and after the application of the mixing process. This is akin to investigating the periodic points or fixed points of the mixing function. In addition, when a fluid is thoroughly mixed, we expect points to diverge from their initial positions, and we expect them to not all converge to a fixed region. If we can demonstrate that most points are not periodic, or asymptotically periodic, and that points in the same neighborhood will on average diverge from each other, then we are essentially demonstrating that under a specific map, the fluid is thoroughly mixed. As we will later see, this concept is fundamentally linked with the theory of chaos and dynamical systems.

# 2 Fluids and Chaos

We can start by introducing the parts of chaos and dynamical systems theory that apply to the field of fluid mixing. Commonly in fluid dynamics, fluid flows are characterized by either particle positions or velocity vector fields. Here we consider the case where fluid flow is periodic, and define a map to be a function that maps each individual position of a fluid particle to the position after one application of the periodic cycle, or advection cycle. In general the differential equation associated with a velocity field $\vec{v}$ is:

$$\dot{x} = \vec{v}(\vec{x}, t) \tag{1}$$

Which has the general solution:

$$x = f_t(x_0) \tag{2}$$

Which denotes the position of a parcel at time $t$, with initial position $x_0$ in the domain $R$. If we take this to be a periodic function with characteristic period $T$, we can then define the mapping of an advection cycle, which will be denoted by a function:

$$S : R \to S(R)$$

$$S(\vec{x}) = f_T(\vec{x}) \tag{3}$$

$$S^n(\vec{x}) = \underbrace{S \circ S \circ S \circ ... \ S}_{n}(\vec{x}) \tag{4}$$

Where $R$ is the domain of the fluid.

The primary question of mixing lies in the efficacy of mixing. We will now formalize a definition of mixing through measure. First, consider a domain

containing two different fluids. The part of the domain that is occupied by fluid A will be denoted $A$ and the part of the domain occupied by fluid B is denoted $B$. Naturally when talking about incompressible fluids and flows, we use the standard Lebesgue measure $\mu(X)$ which gives the volume of some fluid or region $X$. Using this, we can write the volume of fluid B in the region of fluid A after $n$ applications of the map as:

$$\frac{\mu(S^n(B) \cap A)}{\mu(A)} \tag{5}$$

If the fluid is mixing well, we expect that as $n$ increases the volume of fluid B in the region of $A$ will equal the total volume of fluid B over the volume of the domain.

$$\text{As} \quad n \to \infty \qquad \frac{\mu(S^n(B) \cap A)}{\mu(A)} \to \frac{\mu(B)}{\mu(R)} \tag{6}$$

If we normalize the domain such that $\mu(R) = 1$ we can rewrite the equation above such that:

$$\text{As} \quad n \to \infty \qquad \mu(S^n(B) \cap A) \to \mu(B)\mu(A) \tag{7}$$

Another important concept is chaos, which is often synopsized as sensitive dependence on initial conditions. This means that any given starting point $x_0$ and a point that is arbitrarily close to $x_0$ will become separated over time at an exponential rate. This rate is often quantized as the Lyapunov exponent. In two dimensions, the Lyapunov exponent of a given point is the time average of the eigenvalues of the derivative matrix evaluated at each point in the trajectory of an initial condition.

$$h_i(x_0) = \lim_{n \to \infty} \ln \|\lambda_i(x_n)\| \tag{8}$$

Here $\lambda_i(x_n)$ refers to the $i$th eigenvalue of the derivative matrix of $S^n(x_0)$. For an orbit to be considered chaotic we also require that it does not converge to a fixed or periodic point, and does not asymptotically approach an orbit that does converge. A fixed point is one who's position remains constant after any application of the mixing cycle, and a periodic point is one that returns to the same position after a finite number of applications of the map.

Chaotic points in a mixing flow will separate over time. Heuristically we can connect the existence of chaotic flows to good mixing since we can expect particles in general to spread away from each other. Thus the particles that begin in a similar neighborhood will disperse to other locations in the fluid.

Another important concept from dynamical systems theory that applies to fluid mixing is KAM theorem, which predicts that for Hamiltonian systems, in the neighborhood of an elliptic periodic point, there will exist flow structures known as KAM tori. These are formed by quasi-periodic orbits

that form dense tubes surrounding the elliptic point. KAM Tori form invariant surfaces that cannot be crossed by fluid particles and are therefore barriers to mixing. The area surrounded by these tubes is known as an island, due to the fact that particles inside remain separate from the rest of the domain. The proof of their existence is very difficult and often impossible for real world situations, however these types of islands are often observed and connected to the theorem even when not rigorously provable[3].

# 3 Blinking Vortex Problem

## 3.1 Theory

One specific example of fluid mixing can be found in what is known as the Aref-blinking-votex flow. Aref notes in his 1983 paper [1], that when looking at the velocity fields that characterize flows in two dimensional incompressible fluids, effective mixing does not occur in steady, integrable flows. As one of the simplest examples of a non-integrable, time dependent velocity field, Aref introduces the blinking vortex model, which is essentially a Hamiltonian system with one degree of freedom. The velocity field is characterized by two point vortices. At any given point in time, only one point vortex is "turned on" or in dynamical systems terminology, only one map is being applied to the domain at a given time, thus spawning the term 'blinking vortex'.

More formally stated, we can characterize a flow due to a point vortex at the origin through the following velocity field.

$$v_r = 0, \qquad v_\theta = \frac{\Gamma}{2\pi r} \tag{9}$$

The pathlines of this velocity field are clearly denoted by circles about the origin. Similarly, if we set each point vortex at $x = \pm c$, then the pathlines for motion about each vortex will be circles centered at $(\pm c, 0)$.

We can write the Lagrangian coordinates of each fluid parcel using these equations and then define a map, as in Eq. 3, such that each iteration of the map corresponds to a rotation of fixed period $T$. Here we will denote rotation around $+c$ as $S_+$ and rotation around $-c$ as $S_-$. Assuming each is circular and rotating counterclockwise, we get:

$$\int v_\theta d\theta = \int_0^T \frac{\Gamma}{2\pi r}\frac{dt}{r} = \frac{\Gamma}{2\pi r^2}\int_0^T dt = \frac{T\Gamma}{2\pi r^2}$$

$$S_+(x,y) = (c + (x-c)\cos\Delta\theta - y\sin\Delta\theta, (x-c)\sin\Delta\theta + y\cos\Delta\theta) \tag{10a}$$

$$S_-(x,y) = (-c + (x+c)\cos\Delta\theta - y\sin\Delta\theta, (x+c)\sin\Delta\theta + y\cos\Delta\theta) \tag{10b}$$

Where $\Delta\theta = \frac{T\Gamma}{2\pi r^2}$, and we consider one full application of the map to be $S = S_- \circ S_+$. As is common when constructing computational simulations,

we can slightly modify the parameters of the map in order to make them dimensionless. This makes it possible to investigate bifurcations involving only a single parameter. Heuristically we can justify this by saying that in practice, a flow is isomorphic whether the vortexes are strong and far apart, or weak and close together. That being said we can define a new parameter $\mu$ and divide the coordinates by the characteristic length scale of the map, in this case $c$.

$$\mu = \frac{\Gamma T}{2\pi c^2} \qquad [\mu] = \frac{[time][length]^2/[time]}{[length]^2} = [1]$$

$$r = \frac{r}{c} \qquad [r] = \frac{[length]}{[length]} = [1]$$

$$x = \frac{x}{c} \qquad y = \frac{y}{c} \qquad [x], [y] = \frac{[length]}{[length]} = [1]$$

$$\Delta\theta = \frac{\mu}{r^2}$$

$$S_+(x,y) = (1 + (x-1)\cos\Delta\theta - y\sin\Delta\theta, (x-1)\sin\Delta\theta + y\cos\Delta\theta) \quad (10c)$$

$$S_-(x,y) = (-1 + (x+1)\cos\Delta\theta - y\sin\Delta\theta, (x+1)\sin\Delta\theta + y\cos\Delta\theta) \quad (10d)$$

Using this map we can then begin to investigate fixed points and periodic orbits in the domain. There are two main ways of considering the blinking-vortex, the first is exactly as outlined above, with the map being applied to the entire domain during one advection cycle. The second is illustrated in Figure 1. The domain is confined to two bounded annuli with two traverse intersection points. Here the annulus centered around $c$ is denoted $A_1$ and the annulus around $-c$ as $A_2$. Each half of the advection cycle is only applied only on the corresponding annulus. $S_+$ is applied to $A_1$ and $S_-$ is applied to $A_2$. This construction is known as an LTM or Linked Twist Map. The convenience of defining an LTM for the blinking-vortex flow is that it has been proven that on a LTM in two dimensions, a shift map can be defined [2], also known as a Bernoulli shift. When we can define a shift map, we can easily demonstrate the existence of chaos. See Appendix A for more.

The two forms of the blinking vortex will have the same fixed points, given those fixed points are in the area of overlap of the two orbits. When we consider $A_1$ and $A_2$ rotating alternately, fixed points will have trajectories that remain in $A_1 \cap A_2$ after each application of $S_+$ and $S_-$. This will be the same with the unconstrained case, however fixed points do not have to be in the intersection of $A_1$ and $A_2$. Formally we can state that if $(p, q)$ is a fixed point then:

$$S_+(p,q) = (p,-q) \qquad S_-(p,-q) = (p,q) \quad (11)$$

Since $\Delta\theta$ depends on $r^2 = x^2 + y^2$, plugging in these values for equations (7c) and (7d) yields impractically complicated formula's. A geometric argument

can instead be used to describe the fixed points of the map.

Looking at Figure 2, we can easily see that for a fixed point to return to the same location after one advection cycle, the angular position $(\theta_1, \theta_2)$ measured from the x-axis must be equal to 1/2 of the angular displacement caused by each $S_-$ and $S_+$.The most obvious fixed points will occur when an orbit goes directly back and forth between $(p, q)$ and $(p, -q)$ without circling either vortex. This will correspond to the case where $\theta_1 = (1/2)\Delta\theta_1(R_1)$ and $\theta_2 = (1/2)\Delta\theta_2(R_2)$, however we also need to consider the cases where a point will circle all the way around a vortex during one half of the advection cycle. Thus a complete expression of the fixed points of the map can be given by:

$$\left.\begin{aligned}\theta_1 &= \tfrac{1}{2}[\Delta\theta_1(R_1) - 2\pi n(R_1)] \\ \theta_2 &= \tfrac{1}{2}[\Delta\theta_2(R_2) - 2\pi n(R_2)]\end{aligned}\right\} \text{if } q > 0 \tag{12a}$$

$$\left.\begin{aligned}\theta_1 &= \pi - \tfrac{1}{2}[\Delta\theta_1(R_1) - 2\pi n(R_1)] \\ \theta_2 &= \pi - \tfrac{1}{2}[\Delta\theta_2(R_2) - 2\pi n(R_2)]\end{aligned}\right\} \text{if } q < 0 \tag{12b}$$

Where $n(R_i)$ is the number of times a point will circle the vortex for a

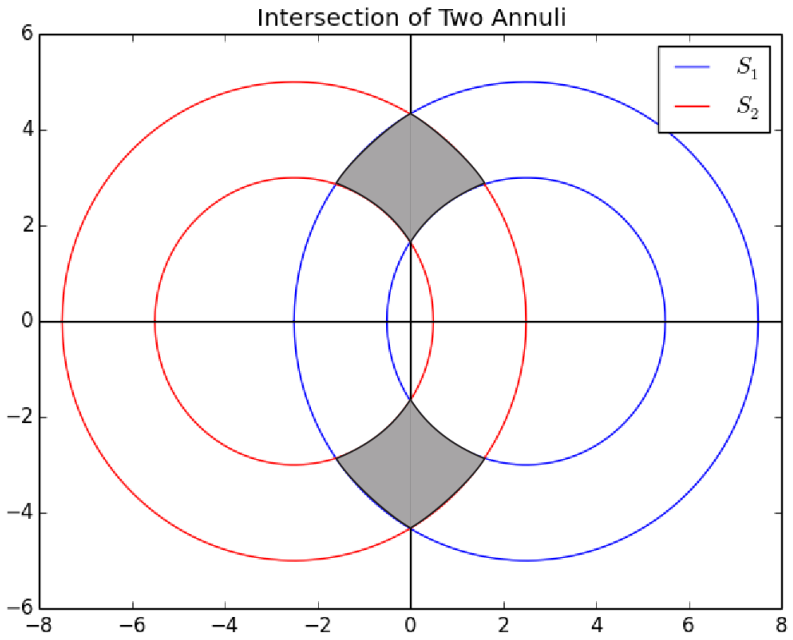


Figure 1: Two Annuli Centered on $c$ and $-c$. By simplifying the flow field this way, it is possible to show that a shift map can be defined on the intersection of the two annuli

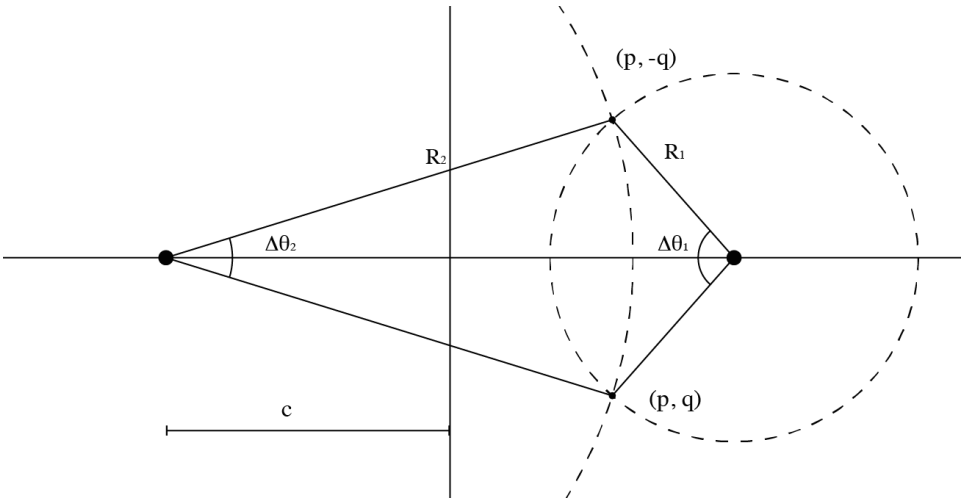


Figure 2: Geometric representation of a fixed point that will oscillate between $(p, q)$ and $(p, -q)$ during one application of the map $S$

defined $R_i$ where each $R_1$ is the radius to $c = 1$ and $R_2$ is the radius to $c = -1$ in dimensionless coordinates. Formally we can define $n(R_i)$ as:

$$n(R_i) = floor\left(\frac{\Delta\theta(R_i)}{2\pi}\right) \qquad i \in \{1, 2\} \tag{13}$$

Using Figure 2 again we can define further restrictions on the angular and radial location of the fixed points. Mainly notice that:

$$R_1 \sin\theta_1 = q = R_2 \sin\theta_2 \qquad c - R_1\cos\theta_1 = p = c + R_2\cos\theta_2 \tag{14}$$

Given these equations presented in (11), we can visualize the locations of fixed points by defining new functions that parametrize $x$ and $y$ coordinates in terms of an arbitrary parameters $\sigma_1$ and $\sigma_2$.

$$\left.\begin{aligned} x_1(\sigma_1) &= 1 - \sigma_1\cos\theta_1(\sigma_1) \\ y_1(\sigma_1) &= \sigma_1\sin(\theta_1(\sigma_1)) \end{aligned}\right\} c = 1 \tag{15a}$$

$$\left.\begin{aligned} x_2(\sigma_2) &= 1 + \sigma_2\cos\theta_2(\sigma_2) \\ y_2(\sigma_2) &= \sigma_2\sin(\theta_2(\sigma_2)) \end{aligned}\right\} c = -1 \tag{15b}$$

Therefore we can graph these two parameters, and where they intersect, $x_1 = x_2$ and $y_1 = y_2$ implying that the corresponding $\sigma_1 = R_1$ and $\sigma_2 = R_2$. This gives us the locations of every local fixed point for the map. Since the map has been made dimensionless, we can then compare the behavior of various fixed points as we alter the parameter $\mu$.

Looking at Figure 2 we can imagine what various bifurcations will look like. For example, as the flow strength increases the two arms closest to the

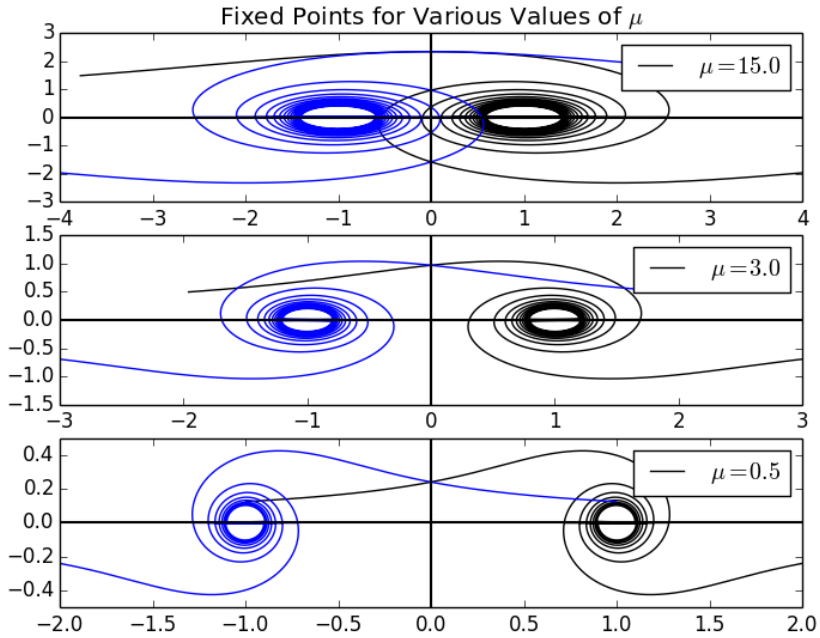


Figure 3: These are three graphs of the fixed point diagrams for various flow strength. The spiral shapes are given by equations 12a and 12b above. Where the two spirals intersect, the conditions are satisfactory for a fixed point or periodic point to exist.

center will cross. When immediately tangent to each other, and touching, they will form a fixed point, however as soon as they overlap, a period doubling bifurcation occurs and two period-two points spawn. This is illustrated in the figure below (Figure 4).

To quantitatively study bifurcations we need to look at the eigenvalues of the map. In general, if $vecf$ is a vector field, then the eigenvalues of the derivative matrix can be found through the characteristic polynomial given by:

$$\lambda^2 - tr(\bigtriangledown \vec{f}) + det(\bigtriangledown \vec{f}) = 0$$

However since the vector fields we are dealing with are all incompressible and thus area preserving, the determinant of the derivative matrix at any point will be one. We can therefore simplify this equation and write the eigenvalues in terms of only the trace of the derivative matrix.

$$\lambda^2 - tr(\bigtriangledown \vec{f}) + 1 = 0 \tag{16}$$

$$\lambda_{1,2} = \frac{1}{2} tr(\bigtriangledown \vec{f}) \pm \sqrt{\frac{1}{2} tr(\bigtriangledown \vec{f}) - 1} \tag{17}$$

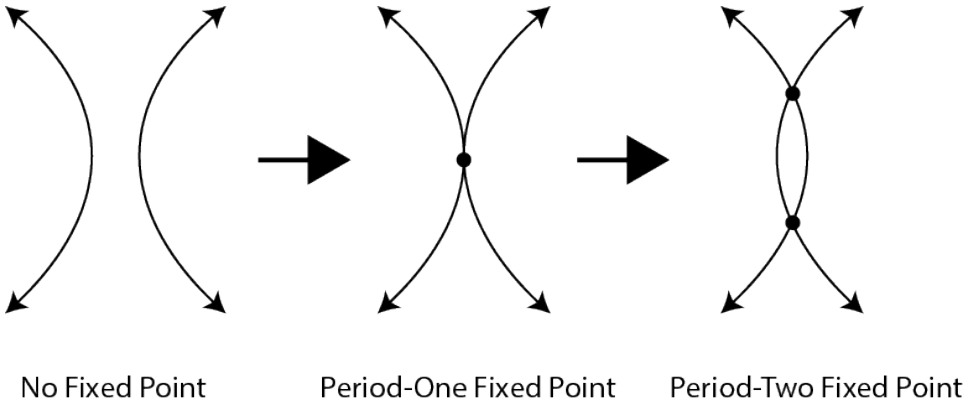


Figure 4: This diagram represents a close-up image of how the arms of the spirals in Figure 3 will behave as the flow strength increases. When two spiral arms cross, a period doubling bifurcation will occur.

In addition the trace of the derivative matrix for our map is equal to the trace of the derivative matrix of $S_+$ multiplied by the trace of the derivative matrix for $S_-$.

$$tr(\bigtriangledown \vec{f}) = tr(\bigtriangledown \vec{f_+}) tr(\bigtriangledown \vec{f_-})$$

Khakhar et al [5] show that for our specified blinking-vortex map, the trace of the derivative matrix is given by:

$$tr(\bigtriangledown \vec{f}) = 2+4\sin(\theta_1+\theta_2)[(\Delta\theta_1\Delta\theta_2-1)\sin(\theta_1+\theta_2)+(\Delta\theta_1+\Delta\theta_2)\cos(\theta_1+\theta_2)] \tag{18}$$

If we just consider the fixed points that do not rotate around the origin, and are above the x-axis, then $n(R_i) = 0$ and $\theta_1$ and $\theta_2$ can be defined as follows:

$$\theta_1 = \frac{1}{2}\Delta\theta(R_1) \qquad \theta_2 = \frac{1}{2}\Delta\theta(R_2)$$

If we further restrict this such that we are only looking at fixed points on the x - axis, then $\Delta\theta(R_1) = \Delta\theta(R_2) = \Delta\theta$ and our formula for the trace can simplify to:

$$2 + 4\sin(\Delta\theta)[(\frac{1}{4}\Delta\theta^2 - 1)\sin(\Delta\theta) + 2\Delta\theta\cos(\Delta\theta)] \tag{19}$$

From our plots in Figure 2 we can numerically calculate the y locations of the fixed points located on the y-axis, determine their radius from either vortex, and use the equation above to calculate their eigenvalues.Figure 5 shows this done for the top fixed point.

If a fixed point has an eigenvalue that is entirely imaginary and of magnitude 1, then it is classified as an elliptic fixed point. KAM theorem states that in the neighborhood of such a fixed point we can expect an island to form. In the next section we use computer simulation to investigate such situations and observe these phenomenon occurring.

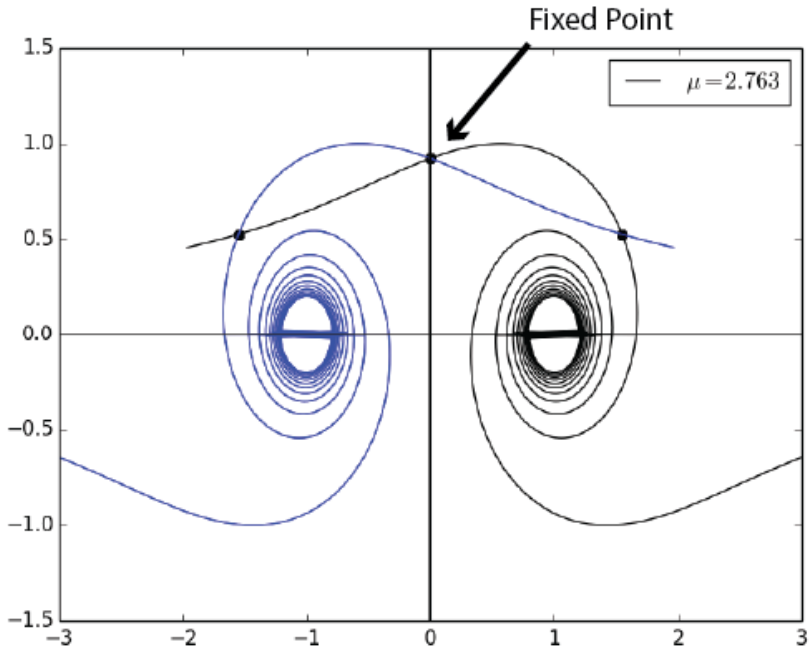


| $\mu$ | $r$ | Trace | $\lambda_+$ | $\lambda_-$ | Type |
|---|---|---|---|---|---|
| **2.0** | 1.24 | - 3.72 | -1.86+1.7i | -1.86-1.7i | Stable Vortex |
| **2.5** | 1.32 | -0.96 | -0.48+1.2*i* | -0.48-1.2*i* | Stable Vortex |
| **2.7** | 1.35 | -0.20 | -0.1 +*i* | -0.1+*i* | Stable Vortex |
| 2.763 | **1.361** | **0.0003** | **≈*i*** | **≈*i*** | **Elliptic** |
| **3.0** | 1.40 | 0.73 | 0.365+0.791*i* | 0.365-0.791*i* | Unstable Vortex |
| **4.0** | 1.52 | 2.61 | 1.85 | 0.75 | Hyperbolic |
| **5.0** | 1.65 | 3.33 | 2.48 | 0.85 | Hyperbolic |
| **6.0** | 1.76 | 3.53 | 2.64 | 0.89 | Hyperbolic |
| **6.3** | 1.793 | 3.55 | 2.65 | 0.89 | Hyperbolic |

Figure 5: Above are the various trace values and eigenvalues for the topmost fixed point and various values of $\mu$. The table classifies each fixed point based off the magnitude of its eigenvalues.

## 3.2 Simulation

The theory defined above tells us what the behavior of the map should be given various parameters. Now we will investigate the blinking-vortex-map computationally. Many of the questions that cannot be answered easily through rigorous mathematics can still be qualitatively analyzed by simulation and modeling. One on the main questions in chaotic mixing is rate at which the domain converges to being perfectly mixed. In the blinking-vortex problem, we have shown two methods of conceptualizing the map. One where the advection cycle is applied to the entire domain, and another where the region mapped is confined to two bounded annuli. As stated before, the benefit of confining the region of studied to the bounded annuli is

that a Bernoulli shift can be applied to the map, and chaotic orbits can be found. In this section, we investigate the differences in the rate of mixing for flows confined to two annuli, and flows calculated over the entire domain.

One of the primary differences between the two functions is that for the map that rotates the entire domain depends, the only parameter is the flow strength $\mu$, however when considering the annuli map, different behaviors of the map can occur with different annuli size and different overlap of each annulus. Wiggins and Ottino demonstrated in their 2004 paper, that optimal mixing in the annuli case occurs when there is maximal overlap between each annulus and yet the two overlapping sections remain disjoint[3]. Thus if we construct our annuli in this way, mixing of the two systems can be compared directly by varying $\mu$. Figure 6 shows these optimally drawn annuli, with $R$ denoting the outer radius and $r$ denoting the inner radius.

$$R = 3c - \epsilon \qquad r = c + \epsilon \tag{20}$$

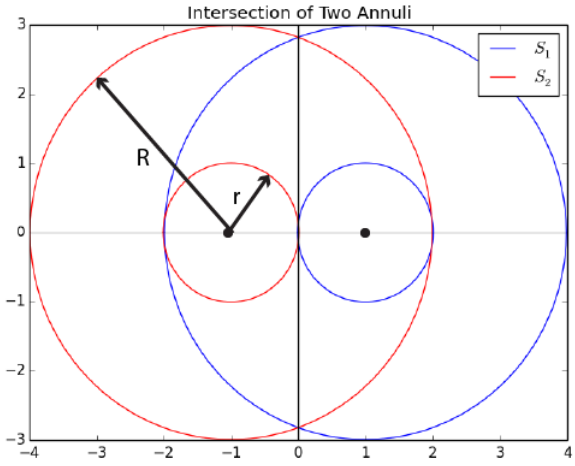


Figure 6: This shows the construction of the two annuli that results in the best mixing. In our simulation, $\epsilon$ is taken to be 0.01 and the centers of each annuli are at $\pm c$

In order to model this system a set of randomly generated points is plotted over the entire area of each annuli. The annulus $(A_1)$ associated with the map $S_+$ is plotted in red and the annulus $(A_2)$ associated with $S_-$ is plotted in blue. In order to measure the rate of mixing, a grid is constructed that overlays the area occupied by the two annuli. After each iteration of the map, the number of red dots and the number of blue dots are counted in each grid square and the following algorithm is used to approximate the

strength of the current mixing.

$$M = \frac{\sum_{i=0}^{N} \frac{|b_i - r_i|}{b_i + r_i}}{N} \tag{21}$$

Where $N$ is the number of squares in the grid partition, $b_i$ is the number of blue points in the $i$th partition, and $r_i$ is the number of red points in the $i$th partition. In this way, as the two regions mix, the value of $M$ will move from 1 to 0 (if moving from completely separated to completely mixed). This model approximates the definition of mixing presented in the first section. Figure [insert reference] shows the various $M$ values for mixed and unmixed iterations of both the annulus map and the full domain map.

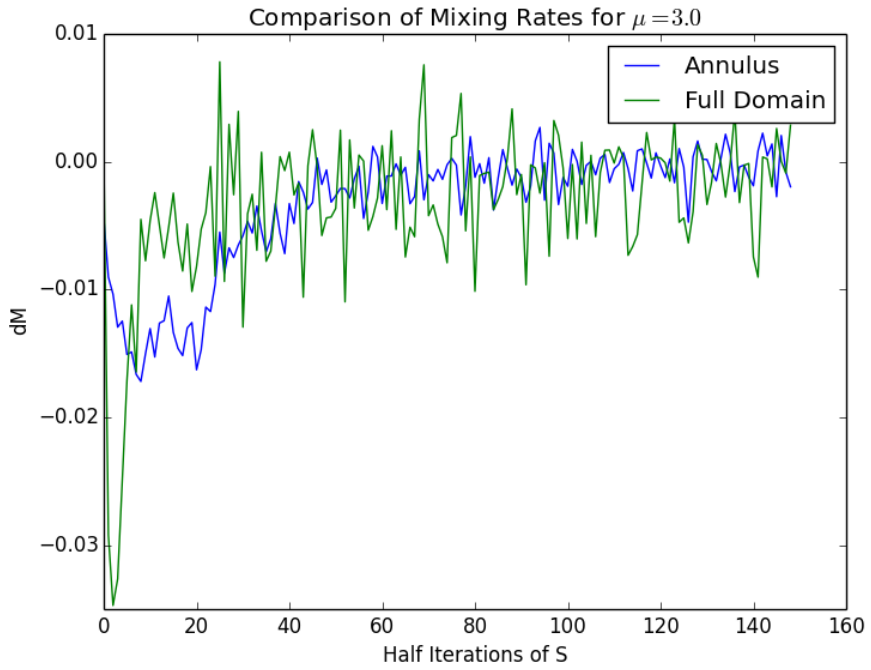


Figure 7: This map represents the average rate of mixing, compiled for both the annulus map and the full field map over 10 runs with the parameter $\mu = 3.0$

Using this value as a measurement of mixing, we can then investigate the rate of mixing in the two maps for corresponding values of $\mu$. Figure 7 shows the derivative of $M$ per advection cycle of each map. As can be seen, the rate of mixing for the same value of $\mu$ is very similar for either map. This tells us that although the annulus map is an idealized version, it approximates the same mixing rate as the full vortex map. During the very beginning the rate of mixing for the annulus drops a bit, but this could

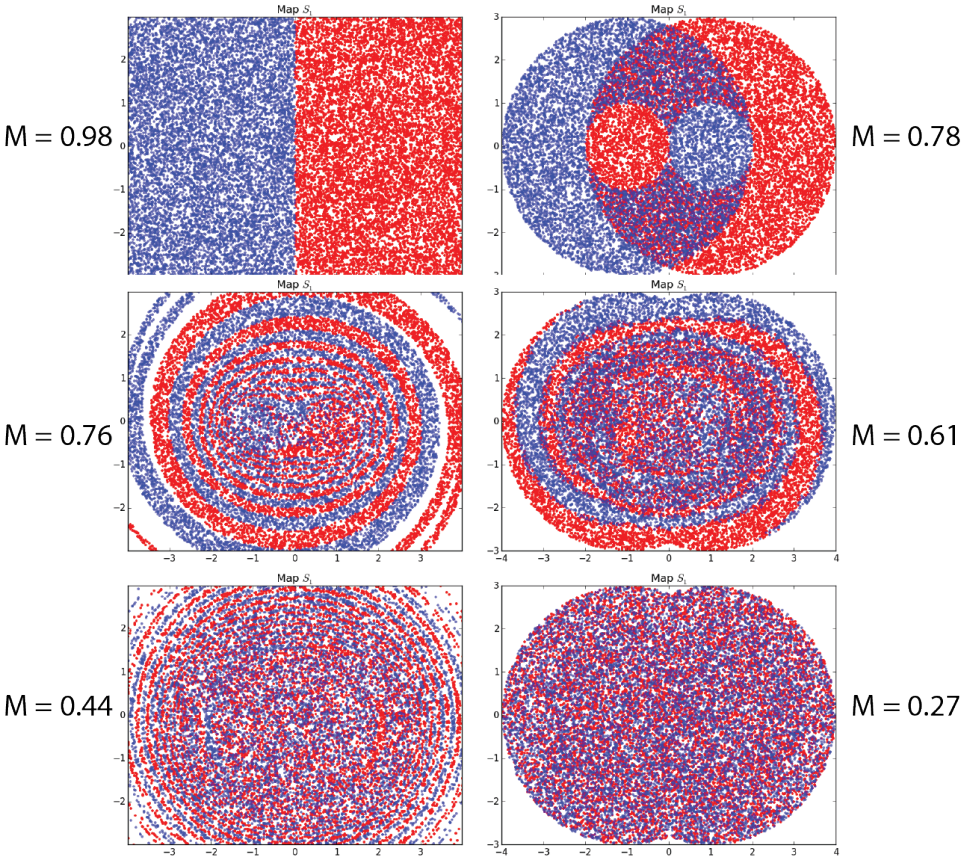


Figure 8: Shown here are various images taken at different stages in the mixing process for each map. Displayed next to each graph is the parameter $M$ which decreases as the two colors become more mixed.

be ruled out if more averages were done. Overall the annulus map seems a good approximation of the mixing rate of the full region map.

Another interesting thing we can computationally observe is the existence of KAM tori in the region predicted in Section 3.1. A simulation was run with exactly the $\mu$ value determined and some of the results are shown in Figure **??**. It is difficult to tell precisely whether an island has formed. Since the value of $\mu$ was found via an approximation, it is also possible that some minor deviation from the actual value causes the island to become unstable and dissipate. Another possibility is that the island exist on a much smaller scale than visible in this simulation. KAM theorem predicts the existence of islands around elliptic fixed or periodic points, but the size of these islands is associated with the nature of each elliptic point.

A final investigation, and a suggestion for further study, is to begin to look for singular chaotic orbits in the map. Figure 10 shows the trajectories

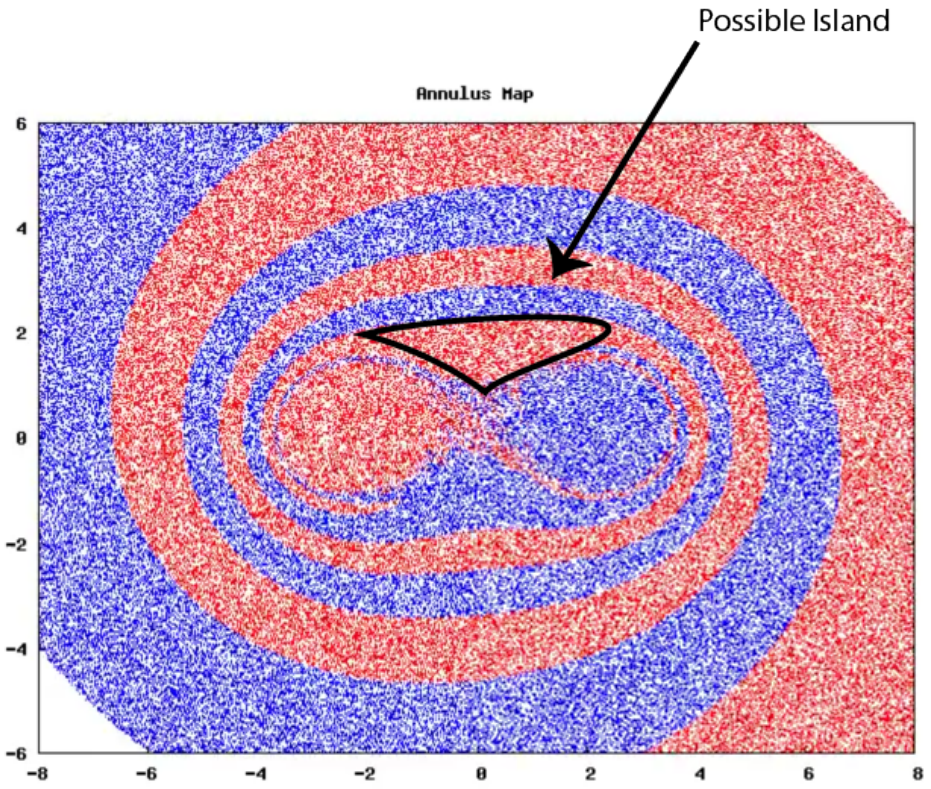


Figure 9: This map attempts to demonstrate an island around an the elliptic periodic point found in Section 3.1 $\mu = 2.673$

of single points in the domain of each of the annulus and full map. From the behavior of the graphs, it seems as though chaos is occurring, however since these are numerical calculations, chaos cannot be confirmed. A further analysis could be done to measure the numerical Lyapunov exponents of all points in the regions of the two vortexes in order to estimate the number of chaotic points in the map.

# 4 Appendix

## 4.1 Bernoulli Shift Map

Defining a Bernoulli Shift map on any dynamical system is akin to defining a symbolic sequence of Markov Partitions. In the specific case of a Bernoulli Shift, a point in the domain of a given map is specified by a bi-infinite sequence.

$$a = (\ldots a_k a_{k-1} \ldots a_{-1}.a_0 a_1 a_2 \ldots a_k a_{k+1} \ldots)$$
$$a_k \in \{0, 1\}$$

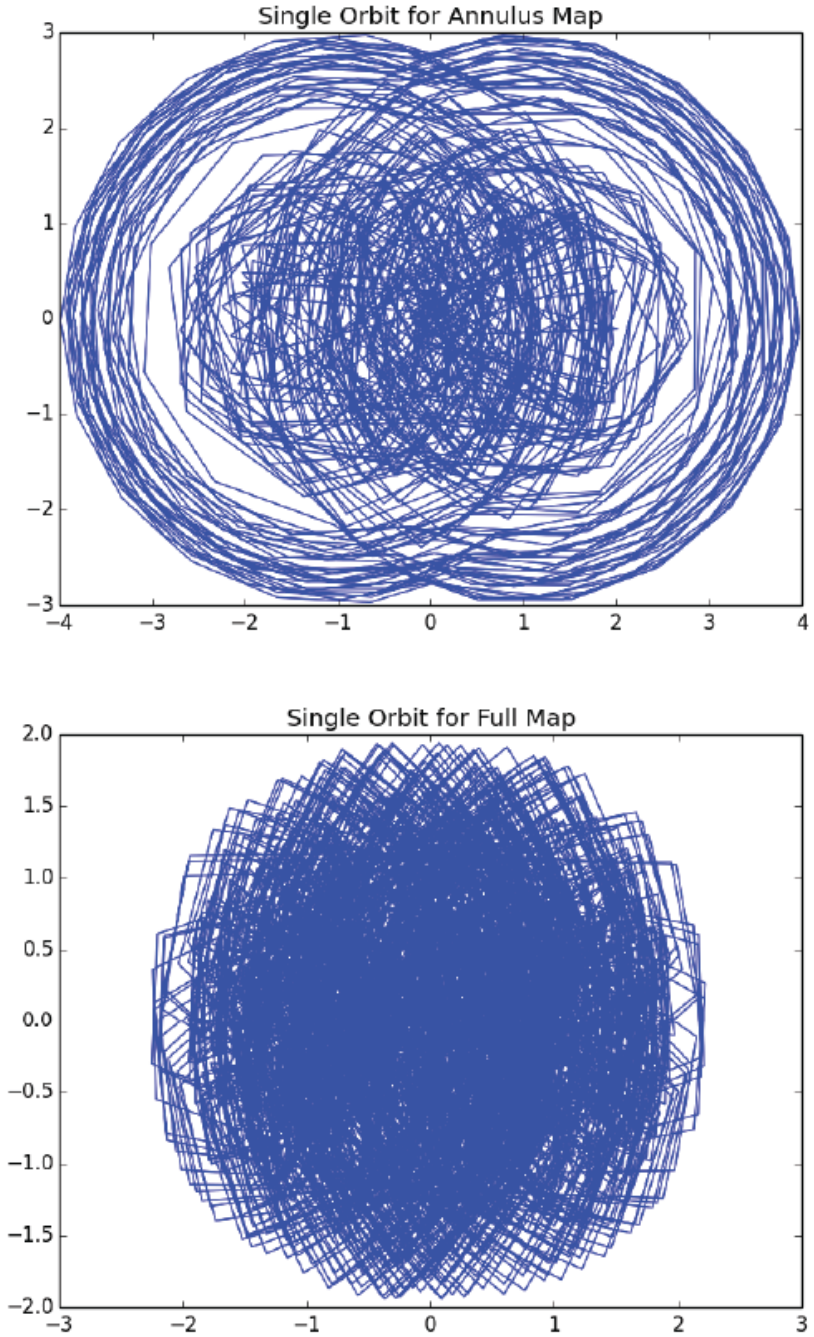


Figure 10: These graphs show the single particle trajectories of a point $x_0 = (0.1, 0.1)$ for both the annulus map and the full field map with $\mu = 3.0$

A shift operation is then defined on $a$ such that:

$$\sigma(a) = (\ldots a_k a_{k-1} \ldots a_{-1} a_0 . a_1 a_2 \ldots a_k a_{k+1} \ldots)$$

In order for a given map to have what is known as the Bernoulli property there must be a one-to-one function that maps $M : \vec{x} \to a$ where $\vec{x} \in \mathbb{R} \times \mathbb{R}$ and $a$ is defined as above. In addition, the shift operator must obey the following:

$$M(\vec{x}) = a \iff M(S(\vec{x})) = \sigma(a)$$

Once a map is known to have the Bernoulli property, there are many things that can easily be proven. For example, every periodic point will correspond to a point whose bi-infinite sequence is periodic. Since periodic sequences of ones and zeros can be mapped to the rational numbers on $[0, 1]$ this tells us that there are countably many periodic points. If the domain is uncountable, and the map has at least one positive Lyapunov exponent, then it tells us that there are uncountably many chaotic points.

An example of a map that has the Bernoulli Property is the skinny baker's map discussed in Section 1. We use a Markov partition to define a symbolic sequence of L's and R's that will represent whether the forward iteration of that point will be in the left side of the map or the right side of the map. An example of this is shown in Figure 11.

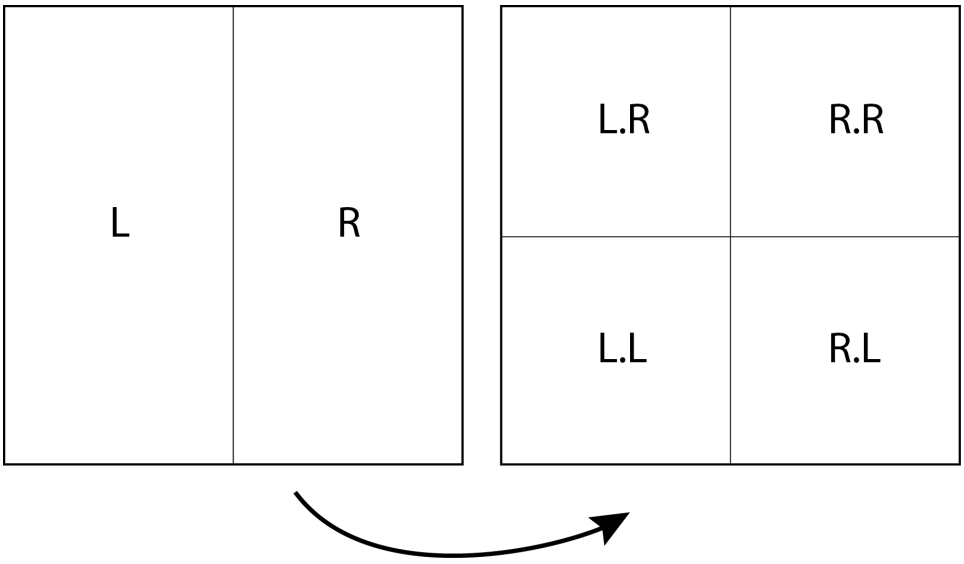


Figure 11: Ever point in the domain $[0, 1] \times [0, 1]$ can be described by the parts that map to it and the parts that it will map to.

Now we can represent every point in the skinny baker's map as a bi-infinite sequence of L's and R's. Consequently, since each L and R can be mapped directly to a 1 or a 0, we can say that the skinny baker's map fits

the criterion for a Bernoulli Shift. Since the L's and R's denote the future and past trajectories of a point, the shift function $\sigma(a)$ will move the decimal over to the right one place, and thus the bi-infinite sequence will represent the next point under the mapping.

One of the interesting things to note about the Bernoulli Property is that often a function that traces every point to a bi-infinite binary series does not need to be explicitly defined. Rather if one can prove that such a function exists, this is generally enough to show the map has all of the associated properties that come with being Bernoulli.

## References

[1] Aref, H. 1984 Stirring by chaotic advection. *J. Fluid Mech.* 86, 1?21.

[2] Burton, R. & Easton, R. 1980 Ergodicity of linked twist mappings. In *Global Theory of Dynamical Systems.* Proc. Int. Conf., Northwestern University, Evanston, IL, 1979, pp. 35?49. Lecture Notes in Mathematics, vol. 819. Springer.

[3] Wiggins, S., Ottino, J. M., 2004 Foundations of chaotic mixing. In *Phil. Trans. R. Soc. Lond. A (2004)* 937-969

[4] Franjione, J. G., Leong, C. W. & Ottino, J. M. 1989 Symmetries within chaos: a route to effective mixing. *Phys. Fluids* A 1, 1772?1783.

[5] Khakhar, D. V., Rising, H. & Ottino, J. M. 1986 An analysis of chaotic mixing in two model systems. *J. Fluid Mech.* 172, 419?451.